The Signature of the Midlatitude Tropospheric Storm Tracks in the Surface Winds

JAMES F. BOOTH

Department of Atmospheric Sciences, University of Washington, Seattle, Washington

LUANNE THOMPSON

School of Oceanography, University of Washington, Seattle, Washington

JÉRÔME PATOUX

Department of Atmospheric Sciences, University of Washington, Seattle, Washington

KATHRYN A. KELLY AND SUZANNE DICKINSON

Applied Physics Laboratory, University of Washington, Seattle, Washington

(Manuscript received 2 February 2009, in final form 23 September 2009)

ABSTRACT

Storm-track analysis is applied to the meridional winds at 10 m and 850 hPa for the winters of 1999–2006. The analysis is focused on the North Atlantic and North Pacific Ocean basins and the Southern Ocean spanning the region south of the Indian Ocean. The spatial patterns that emerge from the analysis of the 850-hPa winds are the typical free-tropospheric storm tracks. The spatial patterns that emerge from the analysis of the surface winds differ from the free-tropospheric storm tracks. The spatial differences between the surface and free-tropospheric storm tracks can be explained by the influence of the spatial variability in the instability of the atmospheric boundary layer. Strongly unstable boundary layers allow greater downward mixing of free-tropospheric momentum (momentum mixing), and this may be the cause of the stronger surface storm tracks in regions with greater instability in the time mean. Principal component analysis suggests that the basin-scale variability that is reflected in the storm-track signature is the same for the free-tropospheric and surface winds. Separating the data based on the boundary layer stability shows that the surface storm track has a local maximum in the region of maximum instability, even when there is no local maximum in the free-tropospheric storm track above the region. The spatial patterns of the surface storm tracks suggest a positive feedback for storm development as follows: 1) an existing storm generates strong free-tropospheric wind variability, 2) the momentum mixing of the unstable boundary layers acts to increase the ocean–atmosphere energy fluxes, and 3) the fluxes precondition the lower atmosphere for subsequent storm development.

1. Introduction

Satellite data and high-resolution general circulation models results show that sharp sea surface temperature (SST) fronts influence the local time-mean and transient dynamics of the atmosphere. Minobe et al. (2008) show that the differential heating across the Gulf Stream has a significant impact on the divergence of the time-mean winds throughout the troposphere. Using surface wind measurements from the Quick Scatterometer (QuikSCAT; Liu 2002), SST measurements from Tropical Rainfall Measuring Mission (TRMM; Simpson et al. 1996), and free-tropospheric winds from European Centre for Medium-Range Weather Forecasts (ECMWF) analyses Simmons and Gibson (2000), Minobe et al. show that the SST has a significant influence on the tropospheric wind fields and precipitation patterns. The annually averaged rain pattern responds to changes in the location of the Gulf Stream in their 50-km-resolution atmospheric general circulation model (AGCM) runs. The SST also influences the transient dynamics of the atmosphere. Nakamura et al. (2008) use an AGCM to show that the SST front in the Southern Hemisphere acts to anchor, or

Corresponding author address: James F. Booth, Department of Atmospheric Sciences, University of Washington, 408 ATG Bldg., Box 351640, Seattle, WA 98195-1640.
E-mail: jbooth@atmos.washington.edu

DOI: 10.1175/2009JCLI3064.1

fix the location of, the wintertime storm track. They theorize that the turbulent heat fluxes from the ocean to the atmosphere on the warm side of the SST front reinvigorate the low-level atmospheric baroclinicity that is removed by wind advection associated with a passing storm. Nakamura and Yamane (2009) show that anomalies in the monthly averaged surface baroclinicity fields in the Gulf Stream region are accompanied by anomalies in the mean fields of the atmosphere up to 50 hPa. Their compositing results suggest that some of the atmospheric anomalies are partially caused by the position or meridional heat transport of the Gulf Stream.

Near the surface, the SST can have a large impact on the surface winds through interaction with the atmospheric boundary layer (for a review, see Small et al. 2008). Nonaka and Xie (2003) show that the SST modifies the boundary layer winds along the Kuroshio Extension. Using QuikSCAT wind measurements, Chelton et al. (2004) show for all oceans that small-scale variability in the wind stress field is partially caused by SST anomalies and associated heat fluxes. This ocean–atmosphere forcing also occurs locally (Sweet et al. 1981) and can be attributed to the coupling of the surface winds and the free-tropospheric winds because of the instability of the boundary layer (Wallace et al. 1989). Following Song et al. (2006), mixing down of momentum due to convective activity in unstable boundary layers is referred to here as the momentum-mixing mechanism. However, this is not the only boundary process associated with SST fronts. Song et al. (2006) show that, during nonstorm conditions, local, thermally forced pressure perturbations near the Gulf Stream SST frontal region are the dominant modifier of the cross-frontal winds. In storm conditions, however, it appears that the momentum-mixing mechanism plays a dominant role (Sampe and Xie 2007).

The signature of extratropical cyclones (ETCs), also called midlatitude storms, in the surface wind field is also connected to the boundary layer stability. Using QuikSCAT satellite winds gridded to ¼° in latitude and longitude, Sampe and Xie (2007) count the occurrence of 10-m wind speeds in excess of 20 m s^{-1}. They state that surface winds of this magnitude are a signature of ETC activity, because surface winds typically reach such speeds only if they are part of a storm. Over the Atlantic Ocean, they find that the high-wind-frequency pattern is very similar to that of the time-mean instability of the atmospheric boundary layer. They stipulate that the high-wind-frequency maxima correspond to locations where the unstable boundary layer allows momentum associated with ETCs to be mixed down from aloft. Over the Pacific Ocean and Southern Ocean, however, the maximum in the Sampe and Xie (2007) high wind frequency occurs west of the region of largest instability, making it difficult to invoke the momentum-mixing mechanism. Although it is clear that the momentum-mixing mechanism explains the occurrence of strong winds in some instances, it does not appear to apply to all ocean basins.

The signature of storm activity can also be evaluated via a storm-track analysis, using temporal filtering to isolate the time scales of baroclinic wave activity (i.e., the synoptic time scale). In this paper, we define baroclinic wave activity as the 2.5–6-day-filtered meridional wind or geopotential height fields, anywhere above the atmospheric boundary layer up to 200 hPa. The storm track is then defined as the region of maximum variance of the specified field. Analysis of filter-based storm tracks has aided in the understanding of the interactions of transient eddies in the atmosphere with the jet stream in the Northern (Lau 1988; Nakamura 1992) and Southern Hemispheres (Lorenz and Hartmann 2001; Nakamura and Shimpo 2004). Hoskins and Hodges (2002, hereafter HH02) show that the patterns that emerge from the filter-based definition of the surface storm track closely resemble the patterns found from feature tracking of the maxima in the meridional winds and temperature anomalies but not necessarily the patterns obtained from feature tracking of the sea level pressure (SLP) minima. Because the path of the SLP minimum is traditionally associated with the path of the midlatitude storm (i.e., the storm's track), HH02's results show that ''storm tracks'' is not the most appropriate term for the patterns captured by the filter-based approach. However, filter-based storm tracks are useful for understanding meridional heat transport associated with transient eddies in the atmosphere. Also, this definition of storm tracks is firmly rooted in the literature. In this paper, storm-track analysis refers to the method of time-filtering gridded data and analyzing the standard deviation of the resulting field.

Joyce et al. (2009) found that yearly anomalies of the time-filtered surface storm tracks in the Northern Hemisphere Pacific and Atlantic Oceans shift coherently with yearly anomalies in the western boundary currents (WBCs) location in the respective basins. Using 22 winters, they examined correlations between the surface storm tracks and the latent and sensible heat fluxes and the WBC variability. They found that there was significant change in the storm-track variability in concert with the changes in the Gulf Stream and Kuroshio Extension at no appreciable seasonal lag, which suggests that the ocean has an influence on the storm-track position. The results of Joyce et al. (2009) encourage a closer look at the surface storm tracks and their connection to the more heavily studied upper-tropospheric storm tracks.

Sampe and Xie (2007) explain that the anchoring of the storm tracks discussed in the opening paragraph

(Nakamura and Shimpo 2004; Nakamura et al. 2008) leads to larger high wind frequency near the regions of strong SST gradients. Although their high-wind-frequency patterns contain broad regions of maxima in each of the ocean basins, corresponding to the storm tracks in those basins, they do not find a tight correspondence between the regions of strong surface winds and the regions of strongest SST gradients in the Pacific or the Southern Ocean. Moreover, because the strongest winds in a storm can occur at different phases of each storm's life cycle and in different sectors at each phase, the high-wind-frequency metric does not provide a complete picture of the relationship between the ETCs, the surface wind field, and the SST fronts.

To supplement the metric developed by Sampe and Xie (2007), here we apply a storm-track analysis to the surface winds to determine the influence of the stability of the atmospheric boundary layer on the structure of variability in the meridional surface winds. These findings are reinforced with a correlation and eigenvalue analysis to determine the relationship between surface winds and free-tropospheric winds. This paper focuses on the three major storm-track regions over the North Atlantic and North Pacific Oceans and the Southern Ocean between Africa and Australia. A comparison of the spatial locations of the maxima in high wind frequency and the surface storm track provides new insights into the development of midlatitude storms and their interaction with the surface ocean.

2. Data and methods

The data used are the 1999–2006 ECMWF operational analyses obtained from the ECMWF data server (ds111.1 for 10-m winds and ds111.2 for 850-hPa winds). The fields are available every 6 h with a grid resolution of 1.125° in latitude and longitude for 10-m winds (i.e., the surface winds) and 2.5° for the 850-hPa winds. The reanalysis is the output of a general circulation model with horizontal resolution T159 (~125 km) and 40 vertical layers. The time period of the analysis overlaps with the availability of QuikSCAT wind measurements. The Eulerian storm tracks derived from the ECMWF data compare well against those derived directly from the QuikSCAT fields (not shown). We chose to use the ECMWF data for the sake of continuity with previous research on Eulerian storm tracks and for the sake of comparing the results with SST, surface air temperature (SAT), and free-tropospheric winds from the same dataset. We define boundary layer instability as SST minus SAT measured at 2 m, with larger positive values indicating more instability.

The use of the QuikSCAT time period did not introduce a significant bias. We compared the variances of the filtered 850-hPa meridional winds over the 8-yr period from 1999 to 2006 with those over the 25-yr period from 1980 to 2005 and found no significant change in the spatial patterns, although the fields were slightly smoother over the longer time period. These differences do not impact the conclusions. In this paper, we focused on the winter months [i.e., December–February (DJF) for the Northern Hemisphere and June–August (JJA) for the Southern Hemisphere], when the storm tracks are strongest and most concentrated (Nakamura 1992; Nakamura and Shimpo 2004).

To isolate the synoptic variability, we filter the data in time, using a 2.5–6-day bandpass filter. The 2.5–6-day time range has been shown to offer an accurate depiction of baroclinic wave activity in the synoptic time scale (Blackmon 1976; Wallace et al. 1988). The filter used in this study is a 10-point Butterworth filter. Note that similar results are found when using a 10-day high-pass filter, and when using a simpler, boxcar filter. To streamline the discussion, we use the ~ symbol to signify the bandpass-filtered winds (e.g., $\tilde{v}_{10}$: 2.5–6-day bandpass-filtered 10-m meridional winds).

To understand the temporal covariability of $\tilde{v}_{10}$ and $\tilde{v}_{850}$, we use principal component (PC) analysis. We examine the correlations between the leading patterns of variability in the 10-m- and 850-hPa-filtered meridional winds. The resulting correlations are all significant within a 95% confidence interval. In each of the storm-track basins, for both $\tilde{v}_{10}$ and $\tilde{v}_{850}$, the first two EOFs explain a large amount of the variance. However, based on the North test for statistical significance (North et al. 1982), the first two modes for each variable have overlapping significance, meaning their spatial patterns are not distinct. This suggests that the leading two modes are together capturing propagating wave activity (Lau and Lau 1990) and that the spatial pattern for either mode is indicative of the wave activity. For each of the storm-track basins, the leading two modes show wave activity characteristic of baroclinic waves (Vera et al. 2002). The EOF patterns seen at 850 hPa are nearly identical to those for meridional winds at 500 hPa, as well as those for the SLP. All of the correlations reported for the PC analysis are statistically significant within a 95% confidence interval.

To aid our understanding of the surface storm track, we bin the filtered winds based on the boundary layer instability. We average the boundary layer stability over a region in which the surface storm track is maximum to create a time series. For the Atlantic, the region is 35°–41°N, 65°–50°W. For the Pacific, the region is 32°–36°N, 145°–160°E. For the Southern Ocean, the region is 39°–45°S, 55°–70°E. For each of these regions, the time-mean boundary layer stability is strongly unstable. There are very few stable days in the average over these regions.

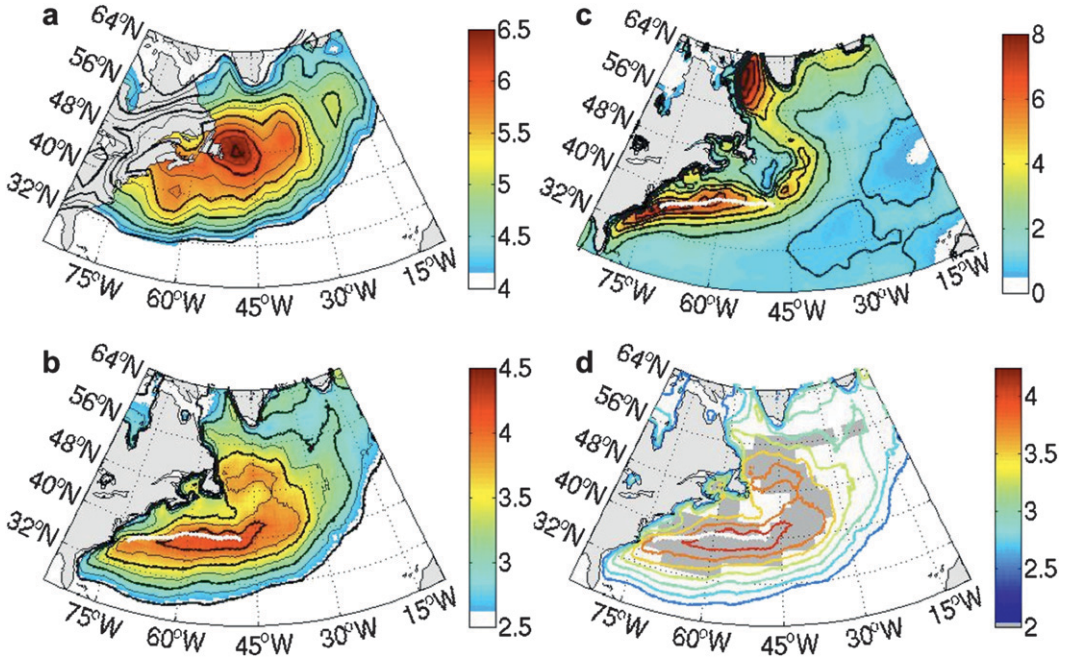

FIG. 1. (a) The free-tropospheric storm track, defined as the standard deviation of the bandpass-filtered meridional winds at 850 hPa. Colors and contours show the same data, with 0.5 (thick lines) and 0.25 m s^{-1} (thin lines) contour intervals. (b) The surface storm track, defined as the standard deviation of the bandpass-filtered meridional winds at 10 m, with colors and contours as in (a). (c) Wintertime mean for air–sea instability (SST minus SAT) of the atmospheric boundary layer. Color and contours show the same data, with contour interval of 1°C. The blue and magenta boxes indicate the locations where the time correlations are calculated (see text). (d) Estimate of the surface storm track as defined in the text (dark gray shading) and surface storm track [contours; same data as shown in (b)]. The mean path of the Gulf Stream, derived from altimetry data, is shown in white in (b),(c), and (d).

After separating the filtered winds based in the stability, we look at the root-mean-square (RMS) of the binned data. This analysis assumes that the amplitude of the filtered winds at each 6-h interval represents a snapshot of the strength of the storm-track variability, which is consistent with the storm-track metric used by Nakamura (1992). Also, this is consistent with our use of the standard deviation definition for the entire winter. Because the wintertime mean of the filtered winds is near zero, the RMS and the standard deviation of the filtered winds over the entire winter are approximately equal. The binning results were robust to changes in the position of the averaging area, the size of the averaging area, and the stability value used for separating the data. Separately, we binned the filtered winds using area averages of the unfiltered wind direction. The results were remarkably similar.

3. Results

a. Gulf Stream region

Over the Atlantic Ocean, the spatial pattern of the standard deviation of $\tilde{v}_{850}$ is typical of the North Atlantic storm track as compared to other methods (reviewed by Chang et al. 2002; Fig. 1a). There is a southwest to northeast tilt, with a maximum near the coast of Newfoundland. The spatial patterns are nearly identical to the patterns of the standard deviation of the bandpass-filtered SLP and 500-hPa meridional winds (not shown), as well as the geopotential height fields at 250 hPa and the meridional winds at 300 hPa (e.g., Chang et al. 2002). The location of the maximum in standard deviation of $\tilde{v}_{850}$ can be interpreted as the region of maximum baroclinic wave activity (Wallace et al. 1988). It is also the location of the strongest northward meridional heat transport by the transient eddies (Blackmon et al. 1977). As discussed in the introduction, it corresponds to the region of maximum intensity for an ensemble of strong wind events, based on feature tracking (HH02). This pattern is referred to here as the free-tropospheric storm track.

The standard deviation of $\tilde{v}_{10}$ (Fig. 1b) shows a pattern that differs from the free-tropospheric storm track. Although both patterns show a southwest to northeast tilt, the locations of their largest values differ. For the filtered surface winds, the largest values occur near 40°N, 70°W and extend along the 40°N parallel, turning north

near 50°W, toward the maximum aloft, whereas there is a minimum near the Grand Banks, around 45°N, 52.5°W (Fig. 1b). We refer to this spatial pattern as the surface storm track.

The momentum-mixing mechanism exerts a strong influence on the spatial pattern of the surface storm track. There is a maximum in the surface storm track along the Gulf Stream, where the boundary layer is usually unstable (because of the warm SST in the core of the Gulf Stream), whereas the surface storm track is weakened north of the Gulf Stream, where the boundary layer is more stable (Fig. 1c). This suggests that downward momentum mixing is enhanced (damped) when the boundary layer is more unstable (stable). To aid in the visualization of the role of momentum mixing in creating the surface storm track, an estimate of the location of the surface storm track is created using the spatial patterns of the free-tropospheric storm track and the mean wintertime boundary layer instability. The estimated surface storm track is defined as grid points (on the 2.5° grid) in which the values of the free-tropospheric storm track and boundary layer instability are in the upper quartiles of their respective distributions for the ocean basin (Fig. 1d). Note that varying the domain used for this calculation requires changes in the cutoff quartile used. However, the results suggest the same relationship: free-tropospheric storm track + unstable boundary layer = surface storm track. There is good agreement between the location of the estimated (in color) and actual (contours) surface storm track (Fig. 1d). The smallest cutoff contour in the actual surface storm track that is covered by the estimated storm track is equal to 3.75 m s^{-1}. The alignment of the actual and estimated storm track suggests that the momentum-mixing mechanism, combined with the structure of the free-tropospheric storm track, explain the spatial pattern of the surface storm track.

The spatial patterns in the wintertime mean boundary layer instability is a result of the interactions of the ocean currents and the advection of cold continental air. There is an instability maximum along the warm flank of the Gulf Stream that wraps to the north near 50°W, following the path of the North Atlantic Current (Fig. 1c). When cold continental air blows over this warm water, the boundary layer is unstable and strong turbulent fluxes of heat occur. These cold air advection events are called cold air outbreaks (CAOs) and usually occur as ETCs exit the Gulf Stream region because of the winds blowing from the northeast behind the cold front of the cyclones (Vukovich et al. 1991). Because these events occur regularly in the winter and consist of strong winds and strong temperature contrasts, the regions of large instability in the time mean correspond with the regions of large turbulent fluxes of heat from the ocean to the atmosphere (Yu and Weller 2007). There is a minimum in instability southeast of the coast of Newfoundland, which is coincident with cold slope water and its source, the Labrador Current (Fig. 1c). Along the shelf, the water is shallow (~50 m) and therefore the ocean can be cooled quickly from top to bottom in the winter. Farther from the coast, the advection of cold water by the Labrador Current brings even colder water into the region (Dupont et al. 2006). In both locations, the instability is minimal and CAOs are not felt as strongly at the surface as over the warm Gulf Stream.

The PC analysis of filtered meridional winds suggests that the 10-m and 850-hPa winds have strong temporal covariability. PC 1 and PC 2 of $\tilde{v}_{10}$ explain 16% and 15% of the variance, respectively; for $\tilde{v}_{850}$, PC 1 and PC 2 explain 17% and 16% of the variance. The location of the maximum (or minimum) within each wave in EOF 1 for $\tilde{v}_{10}$ is located south of the corresponding maximum for $\tilde{v}_{850}$ (Fig. 2), consistent with the patterns seen in the standard deviation fields. The principal components for EOF 1 from 850 hPa and EOF 1 from the surface winds have a time correlation of 0.82. This suggests a strong covariability of the surface and 850-hPa winds for the entire storm-track basin.

The binning results show that, when the boundary layer is most unstable, the surface storm track is strong even when the storm track aloft is not. We separate the data into two bins, one with strongly unstable days and one with the rest of the winter days, using an area average of the boundary layer stability in the region along the Gulf Stream extension (the averaging region is shown in Figs. 3a,d). The top quartile of unstable days has a maximum in the surface storm track along the region of strong instability (Fig. 3c). Meanwhile, the free-tropospheric storm track is relatively weak over this region (Fig. 3b, see the figure caption for details on the contouring). Averaging the unfiltered winds for the strongly unstable days reveals a wind circulation (at both 10 m and 850 mb) that is typical of a large storm exiting the Gulf Stream region, moving toward the northeast: there are northwest to southeast winds west of 50°W, advecting cold continental air over the Gulf Stream and southwest to northeast winds east of 50°W (vectors in Fig. 3a). Thus, the top quartile of instability occurs during the tail end of storms, after their cold fronts have moved through the Gulf Stream region; these wind events also are categorized as cold air outbreaks (Vukovich et al. 1991). The differences in the $\tilde{v}_{850}$ and $\tilde{v}_{10}$ RMS fields for the strongly unstable days (Figs. 3b,c) suggest that the surface storm track can be strong even when the free-tropospheric strong track is moderate. This result is consistent with our postulate that momentum mixing

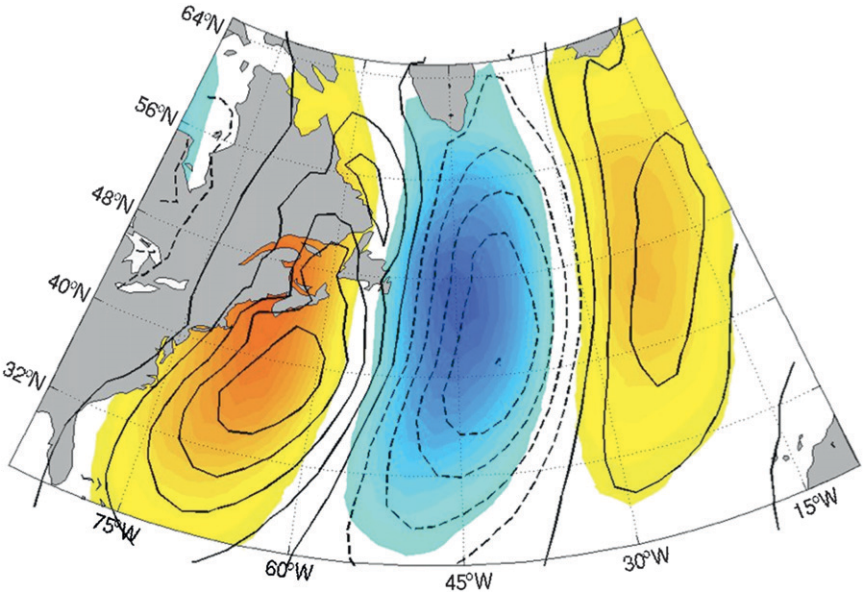

FIG. 2. Leading EOF of the bandpass-filtered meridional winds at 850 hPa (colors) and leading EOF of the bandpass-filtered meridional winds at 10 m (contours).

enhances the surface storm track in regions where the boundary layer is strongly unstable.

The binning results show that the surface and free-tropospheric storm tracks are nearly collocated if we remove the winds associated with the tail end of storms (Figs. 3e,f). The maximum in RMS for the $\tilde{v}_{10}$ and $\tilde{v}_{850}$ are similar, and the slight difference can be partially attributed to the vertical tilt with height that is typical of individual storms (Yin and Battisti 2004). The largest difference is predominantly caused by the land whereby $\tilde{v}_{10}$ decays near the land because surface friction is much greater over land than over water. There is a second region with a large difference, close to the North Carolina coast, in which the surface storm track has a maximum but the free-tropospheric storm track does not; however, Fig. 3d shows that this region also has large instability and thus may be due to momentum mixing.

The strongest free-tropospheric and surface storm track occurs when the leading edge of the storms passes through the Gulf Stream region (not shown). In the leading edge of the storms, winds blow from the southwest to northeast, advecting warm subtropical air northward. This causes the boundary layer in the region over the Gulf Stream to become stable or weakly unstable. Binning the filtered winds about the weakly unstable days reveals a strongly collocated surface and free-tropospheric storm track, and the variability of the winds was very strong (not shown). These events occurred only 10% of the winter days; however, they show that the surface and free-tropospheric storm tracks can have vertical coherence, even when the boundary layer is only weakly unstable.

The surface storm track defined here for the Atlantic basin and the Joyce et al. (2009) vorticity-based storm track have very similar temporal variability. Repeating the Joyce et al. (2009) analysis, we filtered the 10-m relative vorticity for the 2–8-day band. The leading principal components for the meridional winds–based and relative vorticity–based storm tracks have a correlation of 0.91. It is worth noting that this strong correlation occurred only when the EOF analysis was confined to a region south of 50°N. This result makes sense in light of the fact that the bandpass filtering did not have the same effect on the surface relative vorticity field that it did on other atmospheric variables: for the 10-m relative vorticity, the time filtering did not reduce the large variability signal in the Icelandic low region. For all of the free-tropospheric variables, as well as the 10-m winds and sea level pressure, time filtering reduces the variability signal in the region surrounding the Aleutian low. Because of this difference, the EOF analysis of surface relative vorticity using the entire Atlantic basin does not isolate the Gulf Stream basin's storm activity. Instead, it also captures a lot of the winds and storms associated with Greenland. However, the bandpass-filtered vorticity in the Gulf Stream region is analogous to our surface storm track, as evidenced by the sub-50°N EOF analysis, and Joyce et al. used the filtered surface vorticity data from this region for their study.

b. *Kuroshio region*

The spatial pattern of the standard deviation of $\tilde{v}_{850}$ resembles the typically defined Pacific storm track

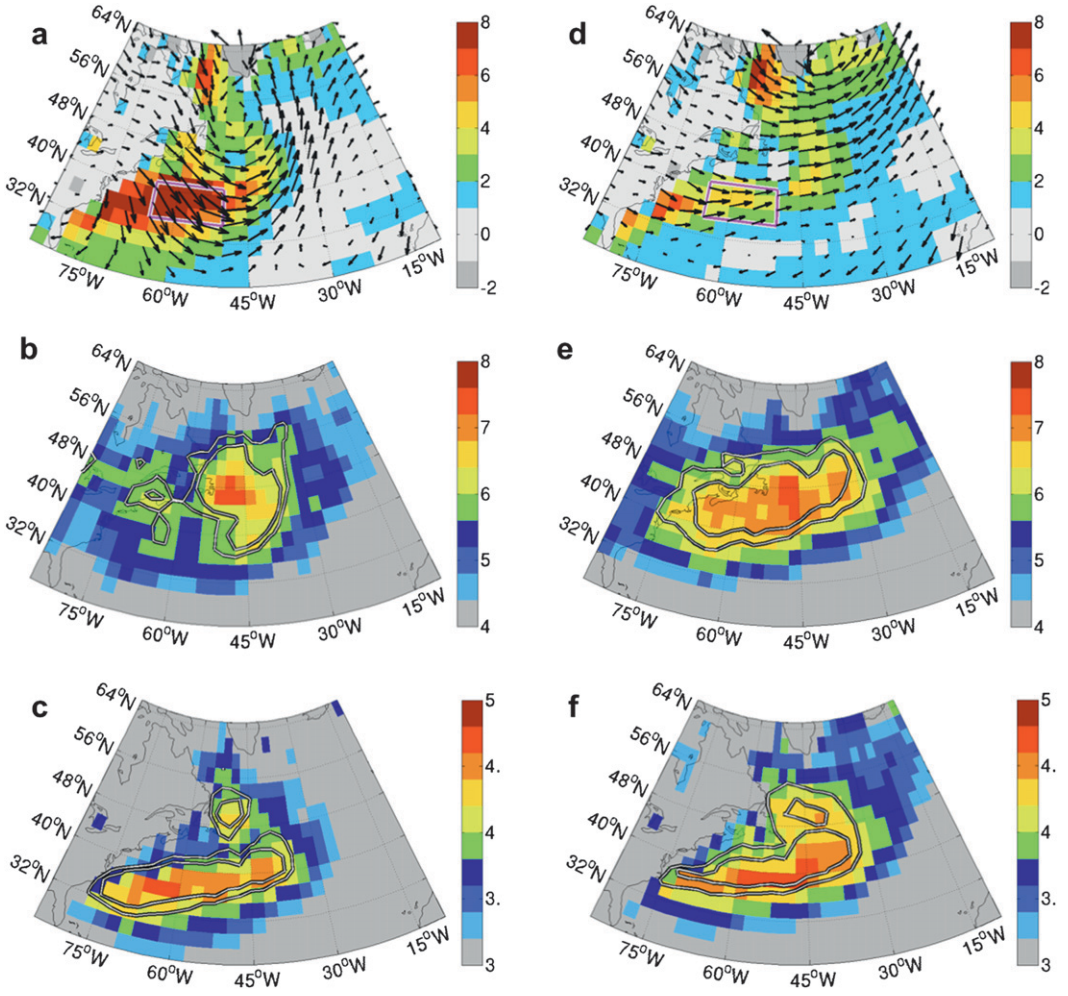

FIG. 3. (a)–(c) The binned days of strongly unstable boundary conditions area averaged over (a),(d) the box shown in magenta. (d)–(f) All other days: that is, the weakly unstable and stable bins. (a),(d) The binned mean of the stability and the unfiltered wind (vectors); average sized vector is 3.5 m s^{-1}. (b),(e) The free-tropospheric storm track, using the RMS [contours: (b) 5.8 and 6.1 m s^{-1} and (e) 6.1 and 6.6 m s^{-1}]. (c),(f) The surface storm track, using the RMS [contours: (c) 3.9 and 4.2 m s^{-1} and (f) 4.1 and 4.4 m s^{-1}]. The contours for figures (b)–(f) correspond to the top 12.5% and top 6% for the basin.

(reviewed in Chang et al. 2002; Fig. 4a). The maximum is located near the center of the North Pacific Ocean (45°N, 180°W). This pattern also appears in the standard deviation of SLP and 500-hPa meridional winds (not shown), as well as other atmospheric fields such as the 250-hPa height field (e.g., Chang et al. 2002). A comparison with the feature tracking results of HH02 shows that, in the Pacific, the storm-track analysis maximum coincides with the region of maximum intensity of the surface lows. Thus, as in the Atlantic, we can consider the maximum in free-tropospheric storm-track activity as representative of the region of strongest baroclinic wave activity.

The spatial pattern of the surface storm track differs from that of the free-tropospheric storm track in the North Pacific as it did in the North Atlantic. The maximum of the surface storm track is south and east of the maximum of the free-tropospheric storm track (Fig. 4b). There is an area of strong variability in $\tilde{v}_{10}$ that extends from the center of the North Pacific all the way to the east coast of Japan. This southwestward extension is not present in the free-tropospheric storm track, but it is coincident with the region of strong boundary layer instability (Fig. 4c). There is considerable overlap between the actual surface storm track and our predicted surface storm track (estimated with the method described in section 3a; Fig. 4d). The smallest closed contour in the actual surface storm track that overlaps the predicted storm track is equal to 4.25 m s^{-1}. From this, we argue that the regions of maximum standard deviation in the filtered surface winds may be explained by a coincidence

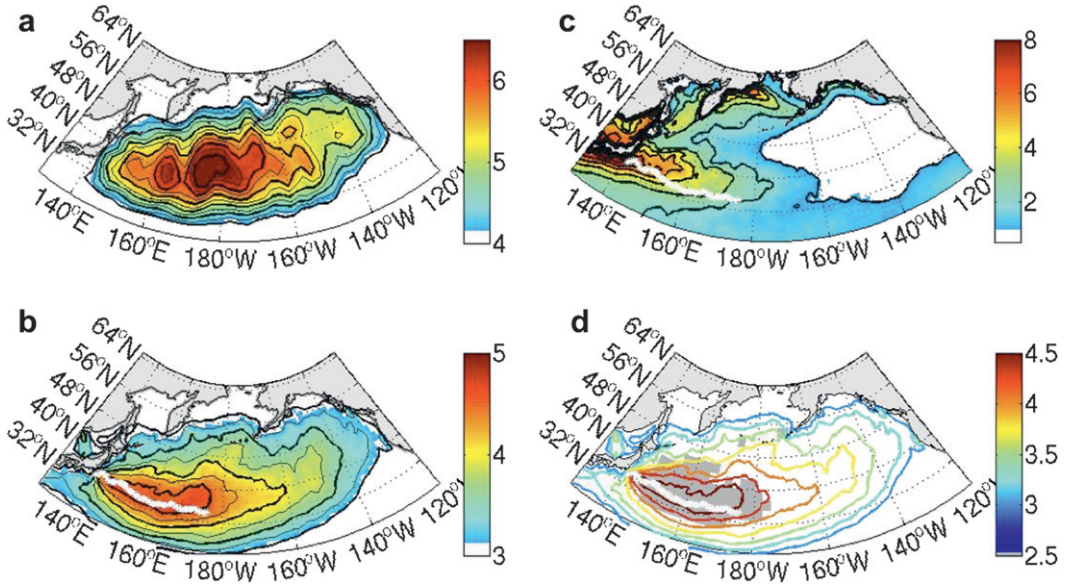

FIG. 4. (a) The free-tropospheric storm track, defined as the standard deviation of the bandpass-filtered meridional winds at 850 hPa, colored and contoured at 0.5 (thick lines) and 0.25 m s^{-1} (thin lines). (b) The surface storm track, defined as the standard deviation of the bandpass-filtered meridional winds at 10 m, with color and contours as in (a). (c) Wintertime mean of the instability (SST minus SAT) of the atmospheric boundary layer, colored and contoured at 1°C intervals. The blue and magenta boxes indicate the locations where the time correlations are calculated (see text). (d) Estimate of the surface storm track as defined in the text (dark gray shading) and actual surface storm track [contours, same data as shown in (b)]. The mean path of the Kuroshio Extension, derived from altimetry data, is shown in white in (b)–(d).

of a strong free-tropospheric storm track and strong surface instability.

The region of large instability in the boundary layer is created by the advection of cold air over the Kuroshio front. As in the Atlantic, cold air outbreaks in the Pacific occur when eastward winds advect cold continental air over the warmer ocean. The instability generated by cold air over warm water is accentuated in the Kuroshio Extension, where the strong western boundary current advects warm water north and east (Fig. 4c). This region corresponds to the area of the largest turbulent heat fluxes (Yu and Weller 2007).

The time series analyses in the North Pacific Ocean show that the major patterns in the winds at both heights vary together in time, consistent with the results found in the North Atlantic Ocean. The maxima (minima) in the wave structure of the EOFs at 10 m are south of their corresponding maxima (minima) at 850 hPa, which is also consistent with the spatial patterns seen in their standard deviations. The first two leading eigenvalues combine to explain 32% of the variability in the 10-m-filtered meridional winds and 33% of the variability in the 850-hPa winds. The correlation of the leading principal components for 10 m and 850 hPa is 0.87. This suggests that, on a basin scale, the leading pattern of variability in the filtered meridional winds at both 850 hPa and 10 m is baroclinic wave activity.

The stability-based binning results for the Pacific are also consistent with momentum-mixing ideas. The top quartile of unstable days show a strong surface storm track in the region of high boundary layer instability, despite the weak free-tropospheric storm track in the region (Figs. 5b,c). The largest instability for a regional average (region is shown in Figs. 5a,d) likely occurs when the winds are advecting cold air south and west. The time mean of the unfiltered winds for the highly unstable days confirm this wind pattern (Fig. 5a). As in the Atlantic, the mean of the binned unfiltered winds picks out a vortical wind pattern, which is somewhat indicative of an individual midlatitude storm circulation, although for the Pacific the circulation pattern is larger than a typical storm (Fig. 5a). In the Pacific, the surface storm track highlights this circulation pattern, with strong variability in the southward winds (centered at 150°E) in the trailing edge of the storm and strong variability in the northward winds (centered at 170°E) at the leading edge of the storm. It is the strong surface storm track in the tail of the storms (where the free-tropospheric storm track is moderate) that contributes to the differences in the surface and free-tropospheric storm-track maxima shown in Figs. 4a,b.

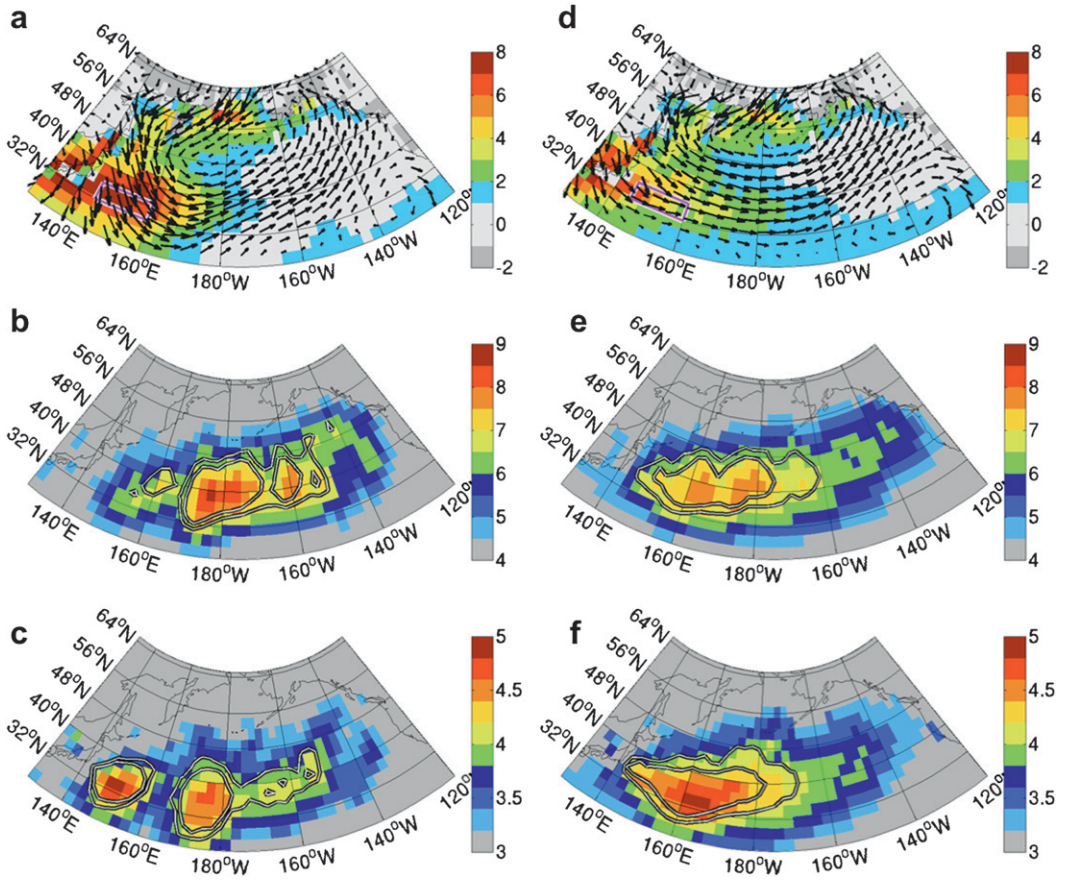

FIG. 5. As in Fig. 3, but contours are (b),(e) 6.5 and 7 m s^{-1}; (c) 3.9 and 4.1 m s^{-1}; and (f) 4.0 and 4.3 m s^{-1}.

As in the Atlantic, the strongest variability in the free-tropospheric and surface storm track occurs when the leading edge of storms is traveling over the western boundary current region. The weakest instability in the boundary layer above the Kuroshio Extension is expected when warm fronts move over the region. Binning the least unstable days (using the area-averaged time series) resulted in a mean, unfiltered wind field typical of a storm whose center is located just east of Japan (not shown). For these weakly stable days, the surface and free-tropospheric storm tracks had their maxima in the same location, and they had the strongest standard deviation (~6 m s^{-1} for the 10-m winds) of any of the stability-based bins that we examined (not shown). This result shows that a strongly unstable boundary layer is not required to mix large amounts of momentum to the surface.

c. Southern Hemisphere

The spatial pattern of the standard deviation of $\tilde{v}_{850}$ reflects the typical Southern Hemisphere storm track south of the Indian Ocean (Nakamura and Shimpo 2004). In the winter (JJA), the Southern Hemisphere storm track is concentrated in the region extending from 10°W to 120°E, with a maximum spanning 12° of latitude centered around 52°S (Fig. 6a). This pattern can be seen in the filtered winds at 500 hPa as well (not shown). Compared to the storm tracks shown in Nakamura and Shimpo (2004), our 850-hPa storm track has a less distinct maximum. However, the maximum at 50°S, 45°E shown in Fig. 6a is the same as the maximum seen in Fig. 1b of Nakamura et al. (2008). A comparison of the filter-based storm track and that of a composite of storms found using feature tracking shows that the Southern Hemisphere winter storm track is coincident with the region of strong northward wind and positive temperature anomalies (Hoskins and Hodges 2005). The Hoskins and Hodges study also shows that this Southern Hemisphere storm track has a genesis region near 42°S between 55° and 75°E and a second genesis region for the same longitude band near the ice edge at 57°S. The dual genesis region leads to a meridional broadening of the region of the eddy activity captured by storm-track analysis and explains why our Southern Hemisphere free-tropospheric storm track (Fig. 6a) is more diffuse than its Northern Hemisphere counterparts.

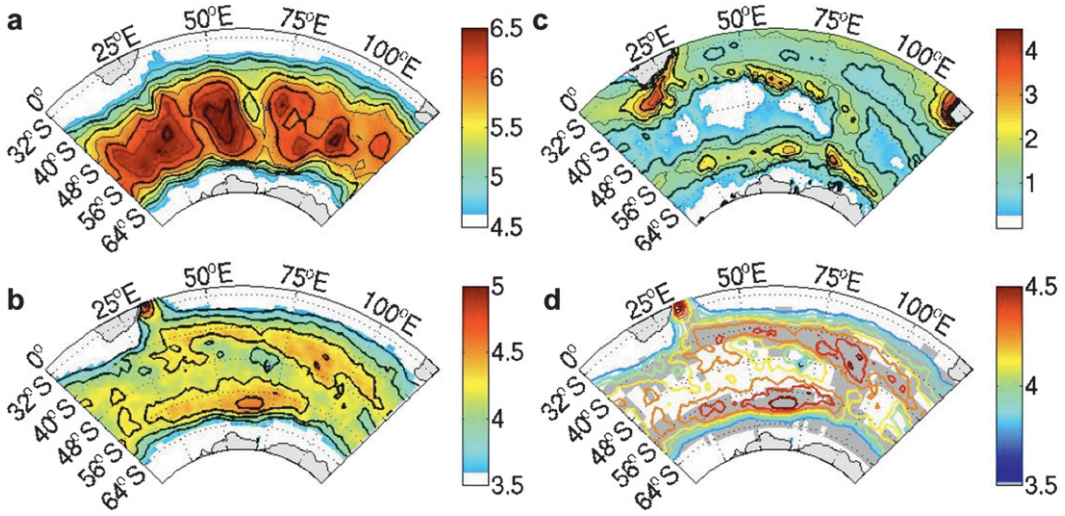

FIG. 6. (a) The upper-tropospheric storm track, defined as the standard deviation of the bandpass-filtered meridional winds at 850 hPa, colored and contoured at 0.5 (thick lines) and 0.25 m s^{-1} (thin lines). (b) The surface storm track, defined as the standard deviation of the bandpass-filtered meridional winds at 10 m, with color and contour as in (a). (c) Wintertime mean instability (SST minus SAT) of the atmospheric boundary layer: color and contours show the same data, colored and contoured at 1°C intervals. The blue and magenta boxes indicate the locations where the time correlations are calculated (see text). (d) Estimate of the surface storm track as defined in the text (dark gray shading) and surface storm track [contours, same data as shown in (b)].

The spatial pattern for the standard deviation of $\tilde{v}_{10}$ appears to reflect the dual influence of the free-tropospheric storm track and the momentum-mixing mechanism in unstable boundary layers. Although the maximum for the free-tropospheric storm track spans 10° of latitude centered around 52°S, the surface storm track has maxima along both 42° and 58°S (Fig. 6b). The latitudinal structure in the surface storm track is coincident with the spatial pattern of time-mean boundary layer stratification (Fig. 6c). The surface storm-track location is estimated by picking out the grid points in which the free-tropospheric storm track and the boundary layer instability are both above their respective mean values (Fig. 6d). For the Southern Hemisphere, weaker thresholds are used for the free-tropospheric storm track and the time-mean stability, because the free-tropospheric storm track is more diffuse than its Northern Hemisphere counterparts and because there are two separate unstable regions in the boundary layer. The resulting pattern has a strong resemblance to the spatial pattern seen in the actual surface storm track.

The large instability along 42°S occurs along the region of the strongest SST front (Nakamura et al. 2008), a region of surface baroclinicity. Feature tracking shows it to be a genesis region for ETCs (Hoskins and Hodges 2005, Patoux et al. 2009). The instability maximum along 60°S is associated with the sea ice edge. It is also a surface baroclinic zone and a genesis region for ETCs in the winter (Hoskins and Hodges 2005). This surface storm-track maximum along the ice edge is distinct from the other surface storm-track maxima, because it does not occur in a region of strong surface currents.

The spatial pattern of the surface storm in the Southern Ocean affirms that the surface wind variability is not some artifact related to contamination of the QuikSCAT data resulting from rainfall (Weissman et al. 2002). For the Atlantic and Pacific basins, the surface storm-track maxima correspond to the regions of heavy precipitation (Simmons and Gibson 2000). However, in the Southern Ocean, the strong surface storm-track regions are not all coincident with the region of maximum precipitation (see Nakamura et al. 2008, Fig. 1a). Therefore, we can say with confidence that the increased variability in the surface winds is not an artifact of noise caused by precipitation in the QuikSCAT data that is assimilated into the ECMWF reanalysis dataset.

The high correlation between the leading principal components of $\tilde{v}_{10}$ and $\tilde{v}_{850}$ suggests that the variability in the surface winds is coincident in time with the variability at 850 hPa. As in the Atlantic, the two leading modes of variability at both 10 m and 850 hPa capture baroclinic wave activity (not shown). The first two modes of $\tilde{v}_{10}$ explain a combined 37% of the variance, whereas the first two modes of $\tilde{v}_{850}$ explain 32% of the variance. The leading principal components have a correlation of 0.80.

The stability-based binning results for the Southern Hemisphere also show an enhanced surface storm track

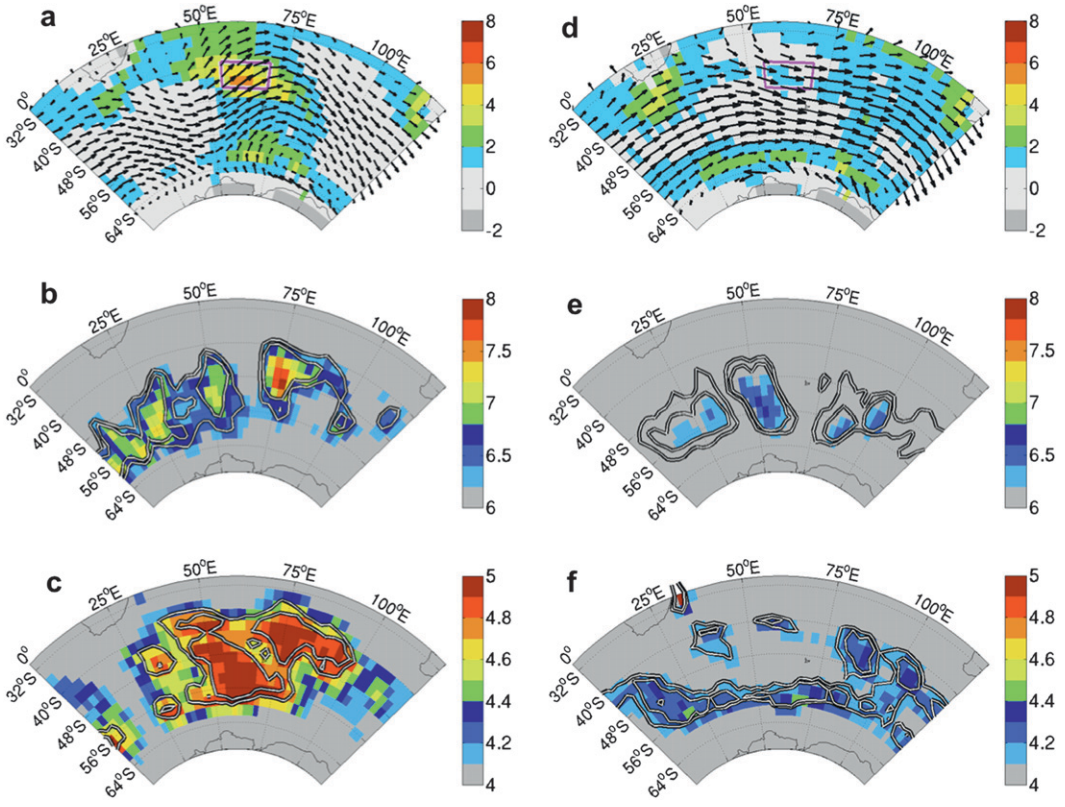

FIG. 7. (a)–(c) The binned days of strongly unstable boundary conditions area averaged over (a),(d) the box shown in magenta. (d)–(f) All other days: that is, the weakly unstable and stable bin. (a),(d) The binned mean of the stability and the unfiltered winds (vectors); average sized vector is 3.0 m s^{-1}. For (d), every other longitudinal vector used is omitted, so that the arrow direction can be seen. (b),(e) The free-tropospheric storm track, using the RMS [contours: (b) 6.4 and 6.7 m s^{-1} and (e) 5.9 and 6.1 m s^{-1}]. (c),(f) The surface storm track, using the RMS [contours: (c) 4.6 and 4.8 m s^{-1} and (f) 4.2 and 4.25 m s^{-1}]. The contours for (b)–(f) correspond to the top 25% and top 12.5% for the basin.

during the most unstable days. The area-averaging region used (Figs. 7a,d) corresponds to the surface storm-track maximum near 42°S and 60°E. This is the location of the maximum in the wintertime mean sensible and latent heat flux (Nakamura et al. 2008). We repeated the binning using the area-averaged stability in the region of the surface storm-track maximum along 57°S and found consistent results: the surface storm track is enhanced compared to the free-tropospheric storm track during the most unstable days, regardless of the strength of the free-tropospheric storm track above it (Figs. 7b,c). The mean field for the unfiltered winds from the unstable bin showed a pattern consistent with storms having recently passed over the area-averaging region (Fig. 7a). Unlike in the Northern Hemisphere, there was not as strong a correspondence between the surface and free-tropospheric storm tracks when the most unstable days were excluded (Figs. 7e,f). This may relate to the greater latitudinal variations in the location of the free-tropospheric storm tracks in this region.

4. Summary and discussion

Storm-track analysis of the surface winds in the North Atlantic reveals a spatial pattern that appears to be a manifestation of the free-tropospheric storm track modified by the spatial pattern of the instability of the atmospheric boundary layer. We theorize that a momentum-mixing mechanism causes the distinct spatial structure differences between the free-tropospheric storm track and the surface storm track. The variability aloft is the primary driver of the variability at the surface, as seen from the strong covariability of the meridional winds, based on principal component analysis. Stability-based binning results show that different patterns in the surface and free-tropospheric storm tracks occur when there is large boundary layer instability, with the surface storm track enhanced in regions of strong instability.

The stability-based binning results show a connection between strongly unstable boundary layers and surface wind variability, but they also show that the enhancement

of momentum mixing by the instability of the boundary layer is not the only factor in determining the surface storm track. For the days in which the boundary layer is stable and weakly unstable, the surface storm-track maximum is coincident with the free-tropospheric storm-track maximum. It is clear from these results that advecting momentum to the surface does not require a strongly unstable boundary layer. Instead, strong variability in the surface winds can occur in two ways: 1) because of some mechanism, such as a storm front, that generates strong wind variability at the surface and in the free troposphere in the presence of moderate momentum mixing (e.g., Stull 1988) and 2) enhanced vertical mixing resulting from the presence of a strongly unstable boundary layer, in which case the free-tropospheric wind variability does not need to be particularly strong.

Although the causality of momentum mixing for the most unstable days cannot be proven with the data available for this study, it provides a likely scenario in the absence of any other more convincing theory. One could imagine that another process determines the surface winds, which in turn would create the strong boundary layer instability. However, not all large instability regions have strong winds, and oceanic processes are known to strongly influence the boundary layer stability. One could also invoke mesoscale structures embedded in fronts or cross-frontal ageostrophic circulations; however, the binning results suggest that the differences between the surface and free-tropospheric storm tracks primarily occur in the lee of the cold fronts, not within frontal regions.

The variance maximum in $\tilde{v}_{10}$ near the Gulf Stream is not an artifact introduced by the filtering procedure. The standard deviation of the unfiltered 10-m meridional winds is also large in the region extending zonally along the Gulf Stream with a minimum over the Grand Banks region (not shown). The differences between the standard deviation for the filtered and unfiltered wind fields are primarily in the northeastern Atlantic. The 2.5–6-day-filtered fields at any height in the atmosphere show substantially less variability than the corresponding unfiltered data for this region near the Icelandic low, which is also considered the storm-track exit region. This is an area in which ETCs tend to clump as one storm overtakes another storm that has stalled (Mailier et al. 2006), and it is the region of maximum low-frequency atmospheric variability (e.g., Thompson and Wallace 2000). In their mature and near-lysisges, storms become more vortical and symmetric about their centers when they are fully developed (Holton 2004). This means that developed storms have more similar wind patterns than developing storms. This may also help to explain why the 2.5–6-day variability is larger near the storm-track entrances when compared to the storm exits, despite the fact that storm winds averaged over the entire storm may tend to be stronger when storms are fully developed.

In the Atlantic basin, the location of the surface storm-track maximum is not representative of the composite of paths of midlatitude storms (not shown). The free-tropospheric storm-track maximum is collocated with the maximum found using the filtered SLP, and it is more indicative of the mean path that individual storms take. From HH02 (their Fig. 6b), it is clear that the path of storms has no local minimum near the coastline or southeast of Newfoundland. Only the surface storm track has a minimum in this location, and that seems to be caused by the momentum mixing in two ways: 1) enhancement of the surface variability over the warmer waters farther away from the coastline and 2) weaker momentum mixing in the strongly stable region southeast of Newfoundland. This region of strong stability is unique to the Atlantic basin.

The storm-track analysis was repeated for the Kuroshio region and produced similar results: the spatial pattern for the surface storm track may be explained by a dual influence of the free-tropospheric storm track and the stability of the boundary layer. In the North Pacific Ocean, the difference between the 850-hPa and surface storm tracks is not as large as in the North Atlantic Ocean for two reasons: 1) the Pacific Ocean lacks the strongly stable boundary layer offshore that characterizes the Atlantic Ocean southeast of Newfoundland and 2) the Pacific Ocean free-tropospheric storm track is located farther east of the coastal region where cold air outbreaks occur. However, the likely role that an unstable boundary layer plays in determining the surface storm track can be seen in the Pacific Ocean (Fig. 4b), because the surface storm track extends west of the maximum in the free-tropospheric storm track, in correspondence with the unstable boundary layer.

For the Southern Ocean, the spatial pattern in the surface storm track is consistent the dual influence on surface winds of the free-tropospheric storm track and the boundary layer stability. There exists a region of strong instability and strong $\tilde{v}_{10}$ in the boundary layer away from the strong surface currents. This reinforces the argument that the primary variability of the winds on the synoptic time scale is driven by variability aloft rather than variability in the SST or ocean surface currents. However, the Southern Ocean storm track is the least consistent of the three basins discussed here, and it warrants further study, especially with regard to the air–sea interactions.

The differences between the surface storm track and the high-wind-frequency metric of Sampe and Xie (2007; discussed in the introduction) suggest that the surface storm track captures the wind variability associated with

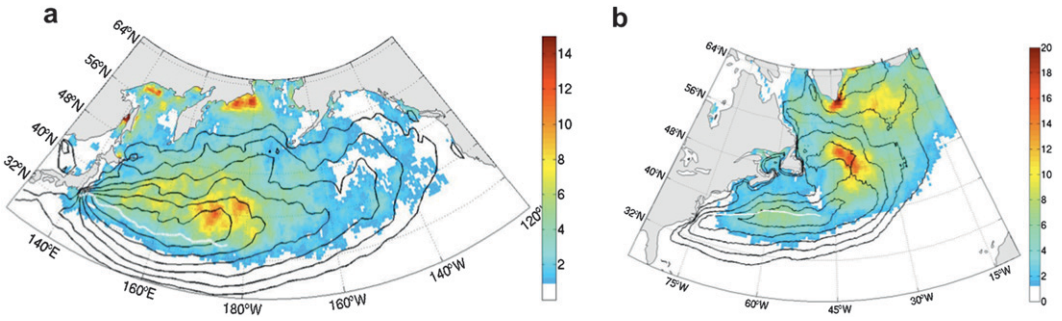

FIG. 8. Frequency of strong wind events based on the unfiltered wind speed at 10 m (color) and surface storm track as defined in Fig. 1 (contours): (a) North Pacific Ocean and (b) North Atlantic Ocean. Units for the color shading are percentage of wind speed greater than 20 m s^{-1} for all days of winter. The contours are at the same interval defined in Fig. 1.

storm development. In the North Pacific, the high wind frequency has a maximum near the center of the ocean basin, in the region of strongest storm intensity (HH02 and Fig. 4a). Because the high-wind-frequency metric measures the strongest storm winds, it captures the storms in their mature phase (for a summary of ETC life cycles, see Holton 2004). In contrast, the surface storm-track maximum is closer to Asia and the Kuroshio Extension (Fig. 8a). This corresponds to the region of ETC genesis (HH02), and it is the entrance of the free-tropospheric storm track (e.g., Chang et al. 2002). A similar difference exists in the Atlantic (Fig. 8b). The high-wind-frequency maximum is close to the maximum in the storm track aloft (Fig. 1a), where storm intensity is a maximum (HH02). In contrast, the surface storm track has its maximum near the entrance of the free-tropospheric storm track, which occurs near the Gulf Stream (e.g., Chang et al. 2002). From our stability-based binning results, we can see that the distinct signature of the surface storm track is partially caused by the winds from the storms exiting the WBC regions (i.e., cold air outbreaks). These events can also be considered the development stages for the next storm that will generate in this region (Vukovich et al. 1991).

The closer agreement between the high wind frequency and the surface storm track in the Atlantic as compared to the Pacific emphasizes the differences in the SST structures in the two basins. In addition, the mean cyclone path is a reflection of the direction of the time-mean winds at the steering level (700 hPa) of the storms (Wallace et al. 1988). In the Atlantic, the time-mean winds at the steering level have a southwest to northeast tilt; in the Pacific, they are more zonal, and this is reflected in the free-tropospheric storm tracks (Figs. 1a, 4a). The direction of the steering winds in the Atlantic causes the majority of storms to travel over the warm waters east of the North Atlantic Current as they are developing. These warm waters in the center of the ocean basin allow momentum mixing to create large values in both the surface storm track and the high-wind-frequency metric. There are no analogous warm waters in the region of the developed storms in the Pacific; as a result, the surface storm track does not extend eastward into the region of the strong high wind frequency.

The time-mean surface winds also contribute to the differences between the surface storm track and the high wind frequency. Surface westerlies in the midlatitudes result from the meridional and vertical momentum fluxes associated with the transient eddies in the atmosphere. These winds are crucial for closing the angular momentum budget of the atmosphere (e.g., Hartmann 1994); however, they are not included in the storm-track analysis (the filtering removes the mean). The mean winds are included in the high-wind-frequency metric, and Sampe and Xie (2007) note their importance. Because the mean winds are strongest near the center of the ocean basin, where the transient eddies fluxes are largest, the high-wind-frequency maximum occurs east of the surface storm-track maximum. However, it is the momentum-mixing mechanism that explains why the surface storm-track maxima occur on the western side of the ocean basins.

The surface storm-track patterns suggest that the Nakamura et al. (2008) theory of SST fronts anchoring the storm tracks may be enhanced by a storm-seeding feedback. Nakamura et al. (2008) show that the differential turbulent surface fluxes on either side of a strong meridional SST gradient reset the surface baroclinic zone that individual storms remove through temperature advection. The rapid reset of the surface baroclinicity allows another storm to form in the region if the upper-level wave conditions are favorable to storm formation. This, in effect, allows the SST gradient to anchor the storm tracks. We have suggested here that the instability of the boundary layer mixes down momentum associated with storms, and this primarily occurs in regions where

the SST is high. This mechanism might be a positive feedback for the storm track: the transfer of momentum down the unstable boundary layer causes stronger winds, which in turn enhance the surface fluxes and precondition the boundary layer for the next possible storm moving through the region. This notion is supported by individual modeling studies of storms that develop over the Gulf Stream region. Reed et al. (1993) show the importance of the latent and sensible heat fluxes during the 24 h prior to the development of the storm. When they turn off the fluxes in their model simulation, the storm is significantly weaker than with surface fluxes turned on. Therefore, it is likely that the enhanced fluxes caused by momentum mixing provide additional moisture and heat to the lower region of the unstable boundary layer, creating a favorable environment for further storm development.

In summary, the location of maxima in the surface storm track suggests the importance of the SST structure in providing an ocean–atmosphere forcing on midlatitude storms. For all three of the ocean basins, the surface storms capture the same temporal variability as the free-tropospheric storms. However, the surface storm-track maximum occurs near the entrance of the free-tropospheric storm track causing the two to have different spatial signatures. We show that this may be an effect of the large boundary layer instability in the entrance regions of the free-tropospheric storm track. However, it is also likely that the stronger boundary layer instability helps in anchoring the position of the free-tropospheric storm tracks, because the surface winds exert direct control on the turbulent energy fluxes between the ocean and the atmosphere.

Acknowledgments. We thank Mike Wallace, Dennis Hartmann, Greg Hakim, and Kevin Rennert for useful conversations on this topic. We also thank the two reviewers and Mike Alexander for their comments, which helped improve the focus and the explanation of results from this research. This research was sponsored by the NASA Ocean Vector Winds Science Team, under Contract 1285662 between the University of Washington and the Jet Propulsion Laboratory.

REFERENCES

Blackmon, M. L., 1976: A climatological spectral study of the 500 mb geopotential height of the Northern Hemisphere. *J. Atmos. Sci.,* **33,** 1607–1623.

——, J. M. Wallace, N. C. Lau, and S. L. Mullen, 1977: An observational study of the Northern Hemisphere wintertime circulation. *J. Atmos. Sci.,* **34,** 1040–1053.

Chang, E. K. M., S. Lee, and K. Swanson, 2002: Storm track dynamics. *J. Climate,* **15,** 2163–2183.

Chelton, D. B., M. G. Schlax, M. H. Freilich, and R. F. Milliff, 2004: Satellite measurements reveal persistent small-scale features in ocean winds. *Science,* **303,** 978–983.

Dupont, F., C. G. Hannah, and D. G. Wright, 2006: Model investigation of the Slope Water, north of the Gulf Stream. *Geophys. Res. Lett.,* **33,** L05604, doi:10.1029/2005GL025321.

Hartmann, D. L., 1994: *Global Physical Climatology*. Academic Press, 411 pp.

Holton, J. R., 2004: *An Introduction to Dynamic Meteorology*. 4th ed. Academic Press, 529 pp.

Hoskins, B. J., and K. I. Hodges, 2002: New perspectives on the Northern Hemisphere winter storm tracks. *J. Atmos. Sci.,* **59,** 1041–1061.

——, and ——, 2005: A new perspective on Southern Hemisphere storm tracks. *J. Climate,* **18,** 4108–4129.

Joyce, T. M., Y. O. Kwon, and L. Yu, 2009: On the relationship between synoptic wintertime atmospheric variability and path shifts in the Gulf Stream and the Kuroshio Extension. *J. Climate,* **22,** 3177–3192.

Lau, K.-H., and N.-C. Lau, 1990: Observed structure and propagation characteristics of tropical summertime synoptic-scale disturbances. *Mon. Wea. Rev.,* **118,** 1888–1913.

Lau, N.-C., 1988: Variability of the observed midlatitude storm tracks in relation to low-frequency changes in the circulation pattern. *J. Atmos. Sci.,* **45,** 2718–2743.

Liu, W. T., 2002: Progress in scatterometer applications. *J. Oceanogr.,* **58,** 121–136.

Lorenz, D. J., and D. L. Hartmann, 2001: Eddy-zonal flow feedback in the Southern Hemisphere. *J. Atmos. Sci.,* **58,** 3312–3327.

Mailier, P. J., D. B. Stephenson, C. A. T. Ferro, and K. I. Hodges, 2006: Serial clustering of extratropical cyclones. *Mon. Wea. Rev.,* **134,** 2224–2240.

Minobe, S., A. Kuwano-Yoshida, N. Komori, S.-P. Xie, and R. J. Small, 2008: Influence of the Gulf Stream on the troposphere. *Nature,* **452,** 206–209.

Nakamura, H., 1992: Mid-winter suppression of baroclinic wave activity in the Pacific. *J. Atmos. Sci.,* **49,** 1629–1642.

——, and A. Shimpo, 2004: Seasonal variations in the Southern Hemisphere storm tracks and jet streams as revealed in a reanalysis dataset. *J. Climate,* **17,** 1828–1844.

——, T. Sampe, A. Goto, W. Ohfuchi, and S.-P. Xie, 2008: On the importance of midlatitude oceanic frontal zones for the mean state and dominant variability in the tropospheric circulation. *Geophys. Res. Lett.,* **35,** L15709, doi:10.1029/2008GL034010.

Nakamura, M., and S. Yamane, 2009: Dominant anomaly patterns in the near-surface baroclinicity and accompanying anomalies in the atmosphere and oceans. Part I: North Atlantic basin. *J. Climate,* **22,** 880–904.

Nonaka, M., and S.-P. Xie, 2003: Covariations of sea surface temperature and wind over the Kuroshio and its extension: Evidence for ocean-to-atmosphere feedback. *J. Climate,* **16,** 1404–1413.

North, G. R., T. L. Bell, R. F. Cahalan, and F. J. Moeng, 1982: Sampling errors in the estimation of empirical orthogonal functions. *Mon. Wea. Rev.,* **110,** 699–706.

Patoux, J., X. Yuan, and C. Li, 2009: Satellite-based midlatitude cyclone statistics over the Southern Ocean: 1. Scatterometer-derived pressure fields and storm tracking. *J. Geophys. Res.,* **114,** D04105, doi:10.1029/2008JD010873.

Reed, R. J., G. Grell, and Y.-H. Kuo, 1993: The ERICA IOP 5 storm. Part II: Sensitivity tests and further diagnosis based on model output. *Mon. Wea. Rev.,* **121,** 1595–1612.

Sampe, T., and S.-P. Xie, 2007: Mapping high sea winds from space: A global climatology. *Bull. Amer. Meteor. Soc.,* **88,** 1965–1978.

Simmons, A. J., and J. K. Gibson, 2000: The ERA-40 project plan. ECMEF ERA-40 Project Rep. Series 1, 63 pp.

Simpson, J., C. Kummerow, W.-K. Tao, and R. F. Adler, 1996: On the Tropical Rainfall Measuring Mission (TRMM). *Meteor. Atmos. Phys.,* **60,** 19–36.

Small, R. J., and Coauthors, 2008: Air–sea interaction over ocean fronts and eddies. *Dyn. Atmos. Oceans,* **45,** 274–319.

Song, Q., P. Cornillon, and T. Hara, 2006: Surface wind response to oceanic fronts. *J. Geophys. Res.,* **111,** C12006, doi:10.1029/2006JC003680.

Stull, R. B., 1988: *An Introduction to Boundary Layer Meteorology*. Kluwer Academic, 666 pp.

Sweet, W., R. Fett, J. Kerling, and P. LaViolette, 1981: Air-sea interaction effects in the lower troposphere across the north wall of the Gulf Stream. *Mon. Wea. Rev.,* **109,** 1042–1052.

Thompson, D. W. J., and J. M. Wallace, 2000: Annular modes in the extratropical circulation. Part I: Month-to-month variability. *J. Climate,* **13,** 1000–1016.

Vera, C. S., P. K. Vigliarolo, and E. H. Berbery, 2002: Cold season synoptic-scale waves over subtropical South America. *Mon. Wea. Rev.,* **130,** 684–699.

Vukovich, F. M., J. W. Dunn, and B. W. Crissman, 1991: Aspects of the evolution of the marine boundary layer during the cold-air outbreaks off the southeast coast of the United States. *Mon. Wea. Rev.,* **119,** 2252–2278.

Wallace, J. M., G.-H. Lim, and M. L. Blackmon, 1988: Relationship between cyclone tracks, anticyclone tacks and baroclinic waveguides. *J. Atmos. Sci.,* **45,** 439–462.

——, T. P. Mitchell, and C. Deser, 1989: The influence of sea surface temperature on surface wind in the eastern equatorial Pacific: Seasonal and interannual variability. *J. Climate,* **2,** 1492–1499.

Weissman, D. E., M. A. Bourassa, and J. Tongue, 2002: Effects of rain rate and wind magnitude on SeaWinds scatterometer wind speed errors. *J. Atmos. Oceanic Technol.,* **19,** 738–746.

Yin, J. H., and D. Battisti, 2004: Why do baroclinic waves tilt poleward with height? *J. Atmos. Sci.,* **61,** 1454–1460.

Yu, L., and R. A. Weller, 2007: Objectively analyzed air–sea heat fluxes for the global ice-free oceans (1981–2005). *Bull. Amer. Meteor. Soc.,* **88,** 527–539.